

$\gamma\gamma$ and γp measurements with forward proton taggers in CMS+TOTEM

J. Hollar, on behalf of the CMS and TOTEM Collaborations

LIP, Lisbon, Portugal

Abstract

The CMS+TOTEM Precision Proton Spectrometer operated for the first time in 2016, collecting data during pp collisions at $\sqrt{s} = 13$ TeV at the CERN Large Hadron Collider. Procedures for the detector alignment, optics corrections, and background estimations were developed, and applied to an analysis of the process $pp \rightarrow p\mu^+\mu^-p^{(*)}$ with dimuon masses larger than 110 GeV. A total of 12 candidate events are observed, corresponding to an excess of $> 4\sigma$ over the background prediction. This constitutes the first evidence for this process at such masses, and demonstrates the good performance of CT-PPS.

1 Introduction

The CMS+TOTEM Precision Proton Spectrometer (CT-PPS) [1] is a joint program of the CMS [2] and TOTEM [3] collaborations, to operate near-beam forward proton detectors in high luminosity proton-proton running at the Large Hadron Collider (LHC). The detectors consist of silicon tracking and fast timing detectors, installed in Roman Pot stations ~ 210 -220m from the P5 interaction region. The detectors are designed to detect the intact protons from “exclusive” production ($pp \rightarrow pXp$), primarily via either $\gamma\gamma$ fusion, or gluon-gluon interactions (with a second screening gluon exchanged to cancel the color flow).

At the LHC, a special class of collisions involves the exchange of quasi-real photons, with the incident beam particles remaining intact. In high energy proton-proton collisions, the spectrum of these $\gamma\gamma$ interactions can extend to the TeV scale, well beyond the range probed at previous colliders. This provides a unique opportunity to study photon interactions in a new energy regime. Detection of the outgoing protons provides strong background suppression and kinematic constraints, making this topology an excellent way to search for new particles and deviations from the Standard Model in low cross section processes (for some recent examples see [4–8]).

1.1 The CT-PPS detectors and 2016 operations

The initial design of CT-PPS called for the installation and commissioning of detectors in 2016, with physics data-taking to start in 2017. However, by making use of the existing TOTEM silicon strip detectors in RP stations at 206m and 214m from CMS, it was possible to begin data taking for physics already in 2016. This required validation of safe Roman Pot insertions at high beam intensities, as well as integration of the data acquisition and reconstruction software between CMS and TOTEM. This was accomplished at the beginning of the 2016 LHC run, and from May the Roman Pots were regularly inserted to 15σ from the beam, with the Si-strip detectors read out through the central CMS DAQ. During the summer of 2016 diamond fast timing detectors were installed in new cylindrical Roman Pots in the 220m region, and began taking data by the end of the LHC proton-proton run.

2 Alignment and optics corrections

2.1 Alignment

The alignment is performed in two steps [10]. First, special low-luminosity fills are used to determine the absolute alignment. This is achieved by inserting the RPs to within 5σ of the beam. By also inserting

vertical RPs, a sample of elastic scattering $pp \rightarrow pp$ events can be collected, allowing alignment with respect to the beam based on the azimuthal symmetry of this process. The horizontal RPs can then be aligned with respect to the vertical RPs, using a subsample of tracks passing through both.

In a second step, the absolute alignment determined in the special fills must be transferred to the case of normal high-intensity fills, where only the horizontal RPs are inserted to a distance $\sim 15\sigma$ from the beam. This is based on matching the measured x distribution of track impact points, under the assumption that the same physics processes contribute to all fills. This results in a set of fill by fill alignment corrections, determined separately for each RP. The total uncertainty of the horizontal alignment procedure is on the order of $150 \mu\text{m}$. The procedure is illustrated in Fig. 1.

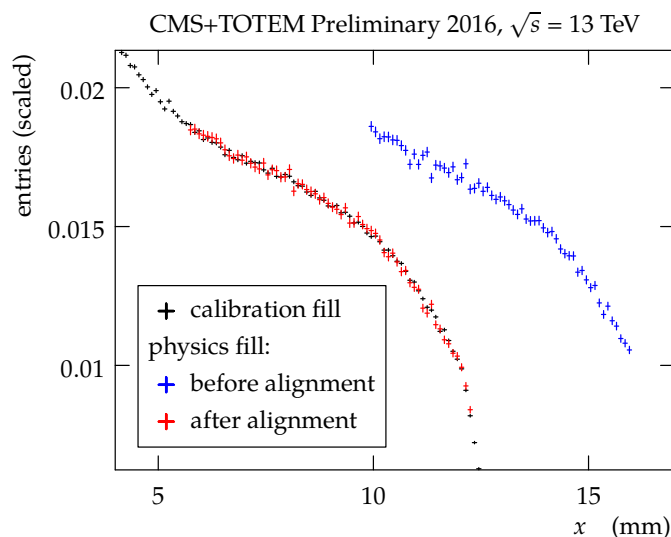


Fig. 1: Distribution of the track impact points as a function of the horizontal coordinate for the alignment fill (black points), a physics fill before alignment (blue points), and after alignment (red points).

2.2 Optics

Having aligned the RPs, a precise determination of the LHC beam optics is required to derive the proton’s fractional energy loss ξ from the measured x coordinates of the tracks. The procedure developed [11] relies on using real data to constrain the elements of the single pass transport matrix $T(s, \xi)$, whose elements are the optical functions of the beam line.

The leading horizontal term in the transport matrix is $x = D_x(\xi) \xi$, where D_x is the dispersion, which has a mild dependence on ξ . The leading term in the vertical plane is $y \approx L_y(\xi) \Theta_y^*$, where $L_y(\xi)$ is the vertical effective length and Θ_y^* is the vertical angle of the proton at the interaction point. The value of $L_y(\xi)$ will go to zero at a particular value of ξ_0 , leading to a “pinch” in the vertical distribution of tracks reconstructed in the RP. By determining the horizontal position of this “pinch”, the value of the dispersion can be solved for as $x_0 \approx D_x \xi_0$ (Fig. 2) where higher-order terms are neglected and included in the systematic uncertainties.

A second independent method is also used to determine the difference in the dispersions in the two LHC beams, by comparing the measured physics proton distribution in the RPs.

2.3 Uncertainties

Given the alignment and optics corrections described in the previous sections, the proton ξ can be reconstructed from the measured x position of the tracks in the strip detectors of the horizontal RPs. For

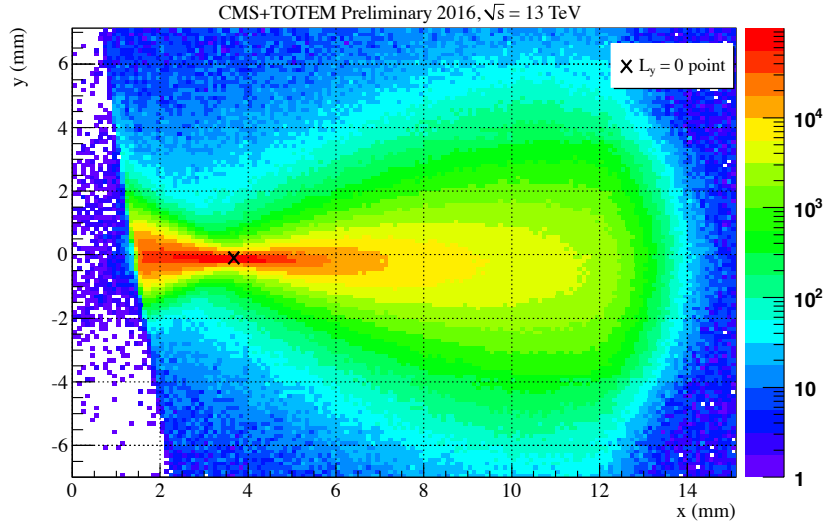


Fig. 2: Distribution of the track impact points measured in RP 210F, in sector 45, in the alignment fill. The point where $L_y = 0$ and its effect in the impact point distribution are shown. The beam center is at $x = y = 0$.

large values of ξ the dominant uncertainty in this determination is 5.5%, arising from the dispersion D_x . Additional uncertainties come from the alignment ($\sigma(x) \approx 150\mu\text{m}$), and the neglected terms in the horizontal terms of the transport matrix ($\sigma(x) \approx 100\mu\text{m}$).

3 Analysis of $\gamma\gamma \rightarrow \mu^+\mu^-$ production

The alignment and optics procedures are then applied to an analysis of $\gamma\gamma \rightarrow \mu^+\mu^-$ production [12], using 10 fb^{-1} of data collected during 2016. In order to increase the acceptance at lower masses, only one detected proton is required. The signal therefore contains a mix of both $pp \rightarrow p\mu^+\mu^-p$ events, and $pp \rightarrow p\mu^+\mu^-p^*$ events, in which one of the protons dissociates into an undetected system p^* .

3.1 Event selection and proton-dimuon matching

An event sample enriched in $\gamma\gamma$ interactions is selected in the central CMS detectors following a procedure similar to that used in earlier studies, in which no detection of the protons was possible. Events are required to have a dimuon vertex with no additional tracks within a veto region of 0.5 mm. The muons are required to have a transverse momentum $p_T > 40\text{ GeV}$, and invariant mass $m(\mu\mu) > 110\text{ GeV}$. In addition, the ‘‘acoplanarity’’ ($1 - |\Delta\phi(\mu\mu)|/\pi$) of the muons is required to be less than 0.009. The selection criteria are chosen such that the expected signal to background ratio after the central detector requirements is > 1 . Because of the high rate of multiple collisions within the same bunch crossing (‘‘pileup’’), the selection is based on information from reconstructed charged tracks and muons, without using information from the calorimeters.

In the case of events in which both protons stay intact ($pp \rightarrow p\mu^+\mu^-p$), the kinematics of the muons and the protons can be precisely related via the expression:

$$\xi(\mu\mu) = \frac{1}{\sqrt{s}}(p_T(\mu_1)e^{\pm\eta(\mu_1)} + p_T(\mu_2)e^{\pm\eta(\mu_2)}).$$

When only one of the two protons remains intact ($pp \rightarrow p\mu^+\mu^-p^*$), the same expression approximately holds when the mass of the dissociating system M_X is small; the deviation becomes comparable

to the experimental dimuon resolution only for masses $M_X \geq 400$ GeV, corresponding to a small fraction of events surviving the zero extra tracks requirement. The signal region is defined to include events where $\xi(\mu\mu)$ and $\xi(\text{RP})$ match within 2σ of their combined experimental resolution.

3.2 Backgrounds and systematics

After the central CMS detector selection, the dominant backgrounds are expected to arise from Drell-Yan $\mu^+\mu^-$ production, and from $\gamma\gamma \rightarrow \mu^+\mu^-$ production with both protons dissociating. These processes can mimic the signal when they occur in the same bunch crossing as a proton from a pileup collision, or a Roman Pot track arising from beam-related backgrounds. A control sample of $Z \rightarrow \mu^+\mu^-$ events is used to estimate the probability of a high mass $\mu^+\mu^-$ event overlapping with an uncorrelated RP track. The $\xi(\mu^+\mu^-)$ distribution in the control region is reweighted to match the distribution predicted by the Drell-Yan simulation for events entering the signal region. Simulation is then used to extrapolate to the number of such events passing the central detector selection on the track multiplicity and acoplanarity. In the case of double dissociation backgrounds, simulated events are normalized to the predicted number passing the central detector selection from simulation, and randomly mixed with protons from the $Z \rightarrow \mu^+\mu^-$ data control sample.

Systematic uncertainties on the background yield include those arising from the statistical uncertainty in the $Z \rightarrow \mu^+\mu^-$ sample used to estimate the backgrounds. For the Drell-Yan background, the modeling of the track multiplicity in the simulation, and the effect of reweighting the $\xi(\mu^+\mu^-)$ distribution, are also considered as systematic uncertainties. For the double dissociation background, uncertainties in the integrated luminosity, and in the theoretical predictions of the survival probability [9], are included as systematic uncertainties. The dominant uncertainties are due to the effect of reweighting the $\xi(\mu^+\mu^-)$ distribution (25%, taken as the full difference between the results with and without reweighting), and the modeling of the track multiplicity distribution (28%, taken as the full difference between data and simulation in the region with 1-5 extra tracks at the dimuon vertex).

The event-by-event uncertainty on $\xi(\mu\mu)$ is estimated to be 3.3%, based on simulation and data-simulation corrections derived from $Z \rightarrow \mu^+\mu^-$ events. The uncertainty on $\xi(\text{RP})$ is taken to be 5.5%, as described in section 2.

The total background estimate, including systematic uncertainties, is 1.47 ± 0.06 (stat.) ± 0.52 (syst.) events, dominated by the Drell-Yan backgrounds.

3.3 Results

The correlation between the predicted $\xi(\mu\mu)$ compared and the measured $\xi(\text{RP})$ is shown in Fig. 3, for the two arms separately. In the region of low $\xi(\mu\mu)$, any signal protons should be outside of the RP acceptance, and only random background correlations are expected. In the region compatible with the RP acceptance, 17 events are observed. Of these, 12 have $\xi(\mu\mu)$ and $\xi(\text{RP})$ compatible within 2σ of the resolution, compared to 1.47 ± 0.06 (stat.) ± 0.52 (syst.) such events expected from the backgrounds only. The significance for observing 12 matching events, including systematic uncertainties, is estimated to be 4.3σ .

In Fig. 4, the signal candidate events are overlaid with an approximate CT-PPS acceptance (including the assumption that the 4-momentum transfer squared $t = 0$) in the dimuon mass-rapidity plane. The events are consistent with the acceptance for detecting one of the two protons in CT-PPS. No events with two protons are seen in the data. The highest mass candidate has $m(\mu\mu) = 341$ GeV, below the region of acceptance for detecting both protons.

4 Conclusions

The CT-PPS project has a broad physics program, including exploration of new physics in $\gamma\gamma$ interactions at very high energies. The detectors operated for the first time in the 2016 LHC proton-proton

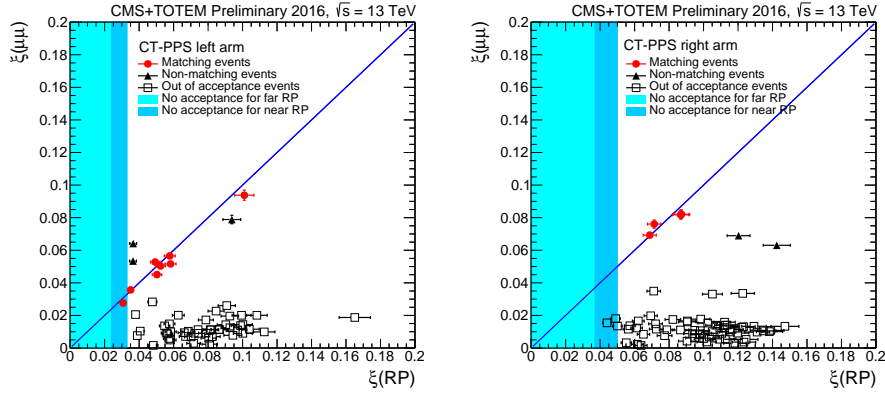


Fig. 3: Correlation between $\xi(\mu\mu)$ and ξ measured in the Roman Pots, for both Roman Pots in each arm combined. The 45 (left) and 56 (right) arms are shown. The light shaded region corresponds to the kinematic region outside the acceptance of both the near and far RPs, while the darker shaded region corresponds to the region outside the acceptance of the near RP. For the events in which a track is detected in both, the ξ value measured at the near RP is plotted.

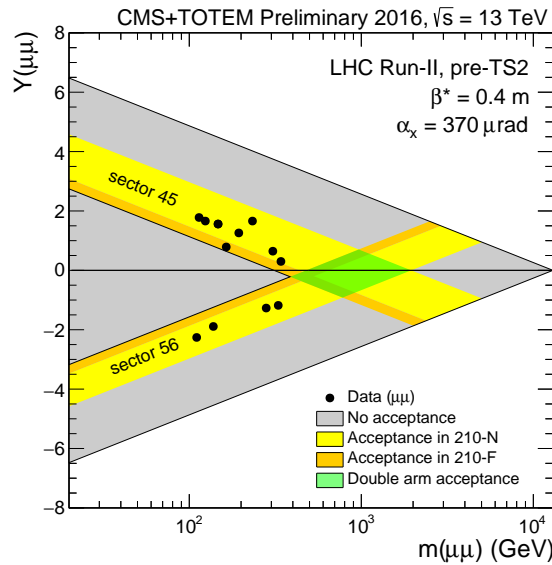


Fig. 4: Expected approximate coverage in the rapidity vs invariant mass plane, overlaid with the observed dimuon signal candidate events.

run, collecting $\sim 15 \text{ fb}^{-1}$ of data. The Roman Pot insertions were validated, the detectors were commissioned, and the data acquisition and reconstruction software were fully integrated between CMS and TOTEM.

Data-driven procedures for the alignment and optics corrections were developed using a combination of special alignment runs, and standard high luminosity data taking. These were applied to an analysis of $\gamma\gamma \rightarrow \mu^+\mu^-$ production with single proton tags. A 4.3σ excess of events with correlated proton and $\mu^+\mu^-$ kinematics was observed with $m(\mu^+\mu^-) = 110\text{-}341 \text{ GeV}$, representing evidence for tagged $\gamma\gamma$ collisions at the electroweak scale. The present data demonstrate the excellent performance of CT-PPS and its potential. With its 2016 operation, CT-PPS has proven for the first time the feasibility of operating a near-beam proton spectrometer at a high luminosity hadron collider on a regular basis.

References

- [1] M. Albrow *et al.*, CERN-LHCC-2014-021, TOTEM-TDR-003, CMS-TDR-13.
- [2] S. Chatrchyan *et al.* [CMS Collaboration], *JINST* **3**, S08004 (2008). doi:10.1088/1748-0221/3/08/S08004
- [3] G. Antchev *et al.* [TOTEM Collaboration], *Int. J. Mod. Phys. A* **28**, 1330046 (2013) doi:10.1142/S0217751X13300469 [arXiv:1310.2908 [physics.ins-det]].
- [4] J. de Favereau de Jeneret *et al.*, arXiv:0908.2020 [hep-ph].
- [5] K. Akiba *et al.* [LHC Forward Physics Working Group], *J. Phys. G* **43**, 110201 (2016) doi:10.1088/0954-3899/43/11/110201 [arXiv:1611.05079 [hep-ph]].
- [6] S. Fichtel, G. von Gersdorff, B. Lenzi, C. Royon and M. Saimpert, *JHEP* **1502**, 165 (2015) doi:10.1007/JHEP02(2015)165 [arXiv:1411.6629 [hep-ph]].
- [7] S. Fichtel, G. von Gersdorff, O. Kepka, B. Lenzi, C. Royon and M. Saimpert, *Phys. Rev. D* **89**, 114004 (2014) doi:10.1103/PhysRevD.89.114004 [arXiv:1312.5153 [hep-ph]].
- [8] S. Fichtel, G. von Gersdorff and C. Royon, *Phys. Rev. Lett.* **116**, no. 23, 231801 (2016) doi:10.1103/PhysRevLett.116.231801 [arXiv:1601.01712 [hep-ph]].
- [9] J. Kaspar, CERN-TOTEM-NOTE-2017-001 (2017) [<http://cds.cern.ch/record/2256296>].
- [10] F. Nemes, CERN-TOTEM-NOTE-2017-002 (2017) [<http://cds.cern.ch/record/2256433>].
- [11] CMS Collaboration *et al.* [CMS and TOTEM Collaborations], CMS-PAS-PPS-17-001, TOTEM-NOTE-2017-003.
- [12] L. A. Harland-Lang, V. A. Khoze and M. G. Ryskin, *Eur. Phys. J. C* **76**, no. 5, 255 (2016) doi:10.1140/epjc/s10052-016-4100-2 [arXiv:1601.03772 [hep-ph]].